



Ductile irons damaging micromechanisms: graphite nodules role investigated by means of image processing procedures

Mauro Cavallini

*Università di Roma "Sapienza", D.I.C.M.A., via Endossiana 18, 00185 Roma
mauro.cavallini@uniroma1.it*

Vittorio Di Cocco, Francesco Iacoviello

*Università di Cassino, Di.M.S.A.T., via G. Di Biasio 43, 03043 Cassino (FR)
v.dicocco@unicas.it, iacoviello@unicas.it*

Daniela Iacoviello

*Università di Roma "Sapienza", D.I.S. "Antonio Ruberti", via Ariosto 25, 00185 Roma
iacoviel@dis.uniroma1.it*

ABSTRACT. Ductile cast irons (DCIs) combine the good castability of gray irons and the toughness of steels. This is due to their peculiar graphite elements shape, obtained by means of a chemical composition control and not by means of extended annealing treatment of white irons (as in malleable irons). Focusing ferritic matrix, different damaging micromechanisms were identified: graphite nodules role seemed to be more complex than the simple "debonding" micromechanism usually considered in numerical simulations.

In this work, a scanning electron microscope (SEM) analysis of metallographically prepared ferritic ductile iron specimens was performed by means of customized image processing procedures, and results were compared with the observed damaging micromechanisms, considering the different graphite nodules solidification mechanisms.

SOMMARIO. Le ghise sferoidali riescono ad offrire una combinazione di proprietà decisamente interessante, essendo caratterizzate dalla elevata colabilità propria delle ghise, e da una buona tenacità, caratteristica degli acciai. Tale risultato è ottenuto grazie alla peculiare forma degli elementi di grafite ottenuta mediante il controllo della composizione chimica e non attraverso lunghi e costosi trattamenti termici, come nel caso delle ghise malleabili. Considerando le ghise sferoidali con matrice ferritica, in precedenti attività sperimentali sono stati identificati diversi meccanismi di danneggiamento, evidenziando un ruolo degli sferoidi di grafite sicuramente più complesso del semplice meccanismo di distacco ("debonding") solitamente utilizzato nelle simulazioni numeriche.

In questo lavoro è stata effettuata una analisi al microscopio elettronico a scansione (SEM) di provini in ghisa sferoidale ferritica preparati metallograficamente utilizzando tecniche di analisi di immagine dedicate, confrontando i risultati con i micromecanismi di danneggiamento e considerando i differenti meccanismi di solidificazione degli sferoidi di grafite.

KEYWORDS. Ductile irons; Image analysis; Graphite nodules.



INTRODUCTION

Up to the first half of the last century, malleable irons obtained by means of an extended annealing treatment of white iron allowed to obtain a combination of good castability and high toughness values. During this heat treatment, cementite decomposes to graphite that precipitates as aggregates in a matrix whose composition (ferrite or pearlite) depends on the cooling cycle from the annealing temperature. The high costs related to the extended annealing treatment and the difficulty to cast sound white iron components limited its utilization. In 1943, in the International Nickel Company Research Laboratory, a magnesium addition allowed to obtain a cast iron containing not flakes but nearly perfect graphite spheres. In 1948, a small amount of cerium allowed to obtain the same result. These cast irons are characterised by a very good combination of overall properties: high ductility (up to more than 18%), high strength (up to 850 MPa and, considering austempered ductile iron, up to 1600 MPa) and good wear resistance. Matrix controls these good mechanical properties and matrix names are used to designate spheroidal cast iron types [1, 2]:

- ferritic ductile irons are characterised by good ductility and a tensile strength that is equivalent to a low carbon steel;
- pearlitic ductile irons shows high strength, good wear resistance and moderate ductility;
- ferritic-pearlitic grades properties are intermediate between ferritic and perlitic ones;
- martensitic ductile irons show very high strength, but low levels of toughness and ductility;
- bainitic grades are characterised by a high hardness;
- austenitic ductile irons show good corrosion resistance, good strength and dimensional stability at high temperature;
- austempered grades show a very high wear resistance and fatigue strength.

DCIs damage micromechanisms analysis is usually mainly focused on voids nucleation and growth due to the matrix-graphite nodules debonding [3-9] and numerous studies provided analytical laws to describe a single void growth, depending on the void geometries and matrix behaviour (Fig. 1).

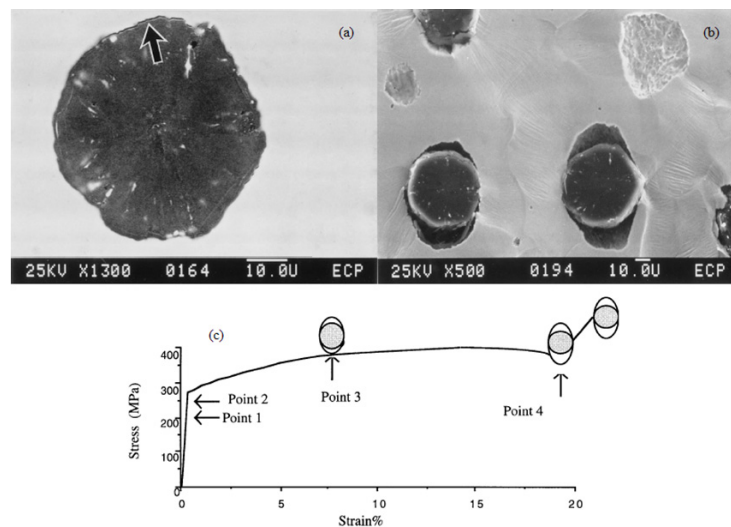


Figure 1: Matrix-graphite nodules debonding evolution during tensile test [3].
 a) decohesion of the interface observed in the SEM at point 2 of the stress-strain curve;
 b) cavity growth around nodules (point 3 of the stress-strain curve SEM observation);
 c) Stress-strain curve recorded during a tensile test.

Berdin et al. [8] proposed that DCIs should be essentially considered as porous materials, graphite nodules being considered as voids in an elastic-plastic matrix. Microcracks in graphite nodules were also observed, but their presence was not considered as important. Damage main micromechanism was identified with graphite – matrix debonding, and all the other mechanisms were considered as negligible. Few slip lines were observed emanating from the equator of the nodules, indicating a local plastic deformation of the matrix and decohesions appeared at the pole cap of the nodules when the macroscopic yield stress was reached. The increase of macroscopic plastic deformation induced void growth in the stress direction, thus forming ellipsoidal cavities inside which nearly undeformed nodules were embedded, failure occurred by shear instabilities linking adjacent voids [10]. According to these experimental results, DCI damage evolution could be summarized considering the following steps:



- Separation between nodular graphite and matrix under low stress.
- Plastic deformation in matrix around nodular graphite.
- Initiation of microcracks in deformed matrix between nodular graphite.
- Linkage of graphite elements by microcracks and formation of larger microcracks.
- Linkage of main crack and selected microcracks to form macrocracks.

Focusing ferritic ductile irons under uniform tensile stress conditions, some experimental results do not agree with the “pure” graphite nodules – ferritic matrix debonding mechanism [10-16]. Elastic stage is confirmed as characterized by a complete absence of cracks or microvoids initiations both in ferritic matrix and in graphite nodules and “pure” ferritic matrix – graphite nodule debonding is only seldom observed. The main ferritic DCI damaging micromechanism consists in cracks nucleation and propagation in the graphite shell coming from the reduced carbon solubility in γ phase (“onion-like” mechanism, Fig. 2). A second damaging micromechanism is sometimes observed developing together with the “onion-like” mechanism: cracks nucleation and propagation corresponding to the nodule center (“disgregation” mechanism, Fig. 3). The importance of this damaging mechanism is dependent on the strain rate value and is probably influenced by the graphite nodule nucleation mechanisms during solidification. Considering the ferritic matrix, the emanation of slip lines corresponding to the nodule equator (lower stress values) is observed, with short cracks that nucleate and propagate corresponding to higher stress values (Figs 2 and 3): final rupture is obtained due to the linkage of cracked graphite nodules by microcracks, with the formation of larger microcracks.

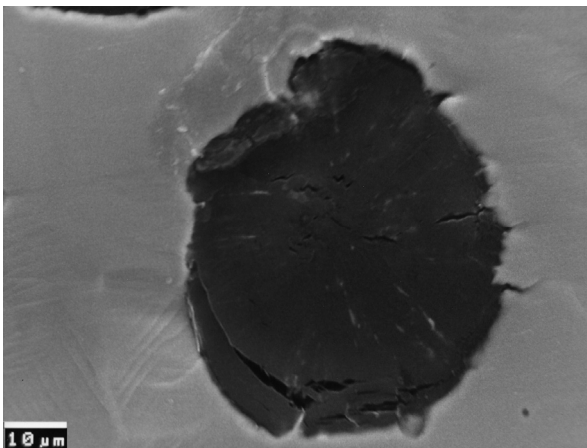


Figure 2: “onion-like” damaging mechanism in graphite nodules; slip lines and microcracks in ferritic matrix.

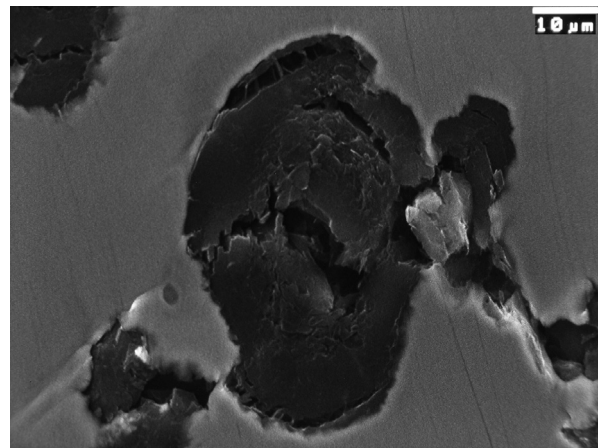


Figure 3: “disgregation” damaging mechanism in graphite nodules; slip lines and cracks in ferritic matrix.

The observed damaging micromechanisms were compared with the graphite nodules nucleation and growth analysed considering a Fe-C-Si ternary phase diagram [2], Fig. 4. Assuming a cooling rate approximately equal to zero and a well inoculated iron, the first solid to crystallize in the investigated hypereutectic DCI is the graphite phase (Fig. 4, point A). Graphite particles volume fraction grows by decreasing the liquid iron carbon content, until temperature reaches the eutectic transformation temperature (Fig. 4, point B).

Austenite grains nucleate and grow in the carbon depleted zone around graphite nodules, generating austenite shells: during eutectic solidification, only austenite is in contact with the liquid iron and graphite nodules grow due to a solid diffusion controlled mechanism of carbon atoms through austenite shells. As carbon solubility decreases in austenite with temperature decreasing, diffusion of C atoms towards graphite nodules continues also after solidification up to eutectoid temperature. Eutectoid transformation implies the transformation of austenite to ferrite: due to the negligible C solubility in ferritic bcc lattice, more C atoms diffuse to nodules. As a consequence of the different “carbon sources” identified describing a ferritic DCI low cooling rate solidification and cooling process, suggesting an homogeneous concentric growth of graphite nodules on nuclei generated from liquid, graphite nodules could be structured as follows:

- a graphite core obtained directly from the melt (C_M);
- a graphite inner shell obtained during eutectic solidification (C atoms solid diffusion through austenite shells, C_E)
- a graphite intermediate shell obtained during cooling (due to C solubility decrease in austenite grains, C_A)
- a graphite outer shell obtained during eutectoid transformation (due to the negligible C solubility in ferritic lattice, C_F).

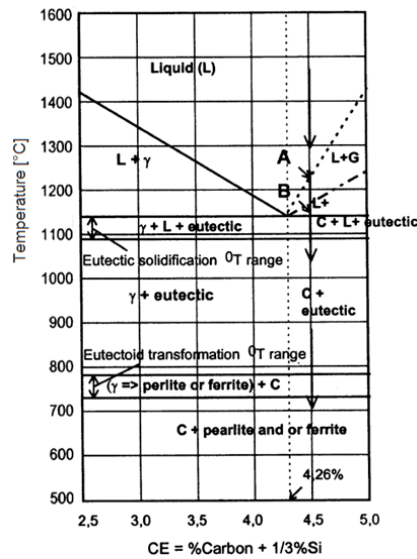


Figure 4: Schematic Fe-Si-C pseudo binary phase (arrows indicate the investigated DCI, C = 3.66%, Si = 2.72%) [2].

On the basis of observed damaging micromechanisms and of the proposed graphite nodules nucleation and growth mechanism, it is possible to hypothesize some differences in the mechanical behaviour of the nodule core compared to its external shield. In this work, these differences were evaluated considering the possibility of a different wear resistance between nodule core and nodule shield. A scanning electron microscope (SEM) analysis of metallographically prepared ferritic ductile iron specimens was performed by means of customized image processing procedures, and results were compared with the observed damaging micromechanisms, considering the different graphite nodules solidification mechanisms.

Image processing is an important instrument that has become more and more important in many different fields for its capability of performing non invasive analysis: it is extensively applied in medicine [17], surveillance [18], robotics [19], just to mention a few. In the last years image analysis has increased its use also in material science; see [20, 21] for some recent papers. Texture analysis is an important topic in image processing and it is considered in many applications. There isn't a unique method that suits for any kind of images, since the possible textures of interest may be very different; basically we may distinguish between statistical, spectral and structural analysis of texture, [22, 23]. In this paper texture analysis in a statistical framework may help in the identification of a "core zone". A preprocessing of the image I by γ -correction is advisable; this operation consists in the power-law expression I^γ . Depending on the value of γ , the resulting image will be clearer or darker.

MATERIAL AND EXPERIMENTAL PROCEDURES

A fully ferritic EN GJS350-22 DCI was investigated (Tab. 1). Graphite elements in the investigated ferritic DCI were characterized by a very high nodularity, higher than 85%, with a volume fractions of about 9-10%.

C	Si	Mn	S	P	Cu	Cr	Mg	Sn
3.66	2.72	0.18	0.013	0.021	0.022	0.028	0.043	0.010

Table 1: Ductile cast iron EN GJS350-22 chemical composition (100% ferrite).

DCI specimens were metallographically prepared and SEM observed. Two different analysis procedures were considered in order to analyse graphite nodules:

- a 3D fracture surface reconstruction procedure. Corresponding to the same specimen position, a stereoscopic image is obtained performing an eucentric tilting around the vertical axis and capturing two different images, with a tilting angle equal to 6° (tilting results in a static center point in the image, Fig. 4). 3D surface reconstruction was performed using the Alicona MeX software and profile evolution was analysed corresponding to graphite nodules.

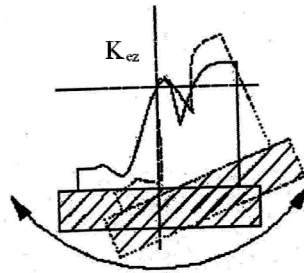


Figure 4: Eucentric tilting.

- a customized image processing procedure aimed to the identification of a nodule “core zone”, with a different characteristics if compared to a nodule “shield zone”.

The procedure adopted to identify the nodule “core zone” is based on the concept of texture [22]. There isn't a unique definition of texture; roughly speaking it describes spatial relations between pixels in image, for example the coarseness or the fineness. In texture analysis one of the most difficult aspect is to define the properties that adequately describe the characteristics of the texture. In the considered images the main texture properties that will be considered are the Entropy, the Uniformity and the Contrast.

For the reader convenience we briefly recall the definition of these quantities. Let z denotes the gray level, L a chosen number of distinct gray levels, $p(z_i)$, $i = 0, 1, 2, \dots, L-1$ the corresponding histogram and consider a chosen sub domain, for example a square of size q . The average entropy measure is defined as follows:

$$\bar{E} = -\sum_{i=0}^{L-1} p(z_i) \log_2 p(z_i)$$

For constant images the value of Entropy is equal to zero; it is a measure of variability of the gray level.

The Uniformity is given by:

$$\bar{U} = \sum_{i=0}^{L-1} p^2(z_i)$$

It is maximum in the regions in which all gray levels are equal.

The Contrast is given by the standard deviation of the pixels intensity :

$$\bar{C} = \sqrt{\frac{(I - I_m)^2}{q^2 - 1}}$$

where I_m is the mean value of the image I in the considered sub domain.

Therefore, where the images are constant the entropy is equal to zero, the uniformity assumes its maximum value and the contrast is minimum.

Let us go back to our application. The image may divided into non overlapping squares with side of length q . In each of these sub domains the above quantities Entropy, Uniformity and Contrast are evaluated. The obtained constant values \bar{E} , \bar{U} and \bar{C} are assigned to each pixel constituting the considered $q \times q$ square and are computed for each square in which the image has been tiled. Therefore we obtain three new matrices, the matrices of Entropy (E), of Uniformity (U) and of Contrast (C). Let us consider the weighted sum of the Uniformity matrix, the Entropy matrix and the Contrast matrix:

$$f = \alpha_1(1-U) + \alpha_2 E + \alpha_3 C, \quad \alpha_1, \alpha_2, \alpha_3 \in R$$

This texture function will assume its maximum value where the gray level of the image varies more than in other regions. A binarization operation allows to enhance the zones of the image in which the core zone is present; moreover, taking into account that the zone interesting for our purpose should be inside the specimen, by logical operation it may be



retrieved. This region may be completely described by its morphological characteristics, like, for example, the area, the centroid, the eccentricity and so on.

Results were compared with the analysis of the graphite nodules solidification process in the investigated DCI. Considering a Fe-C phase diagram with a Si content close to 2.72% (Fig. 5), and assuming a cooling rate approximately equal to zero, graphite volume fractions obtained in the different solidification and cooling stages has been evaluated by means of a concentric homogeneous spherical growth model. The corresponding graphite nodule radiuses R [16] are:

- $R_{C_M} = 0.38 R_{nodule}$
- $R_{C_M + C_E} = 0.89 R_{nodule}$
- $R_{C_M + C_E + C_A} = 0.95 R_{nodule}$

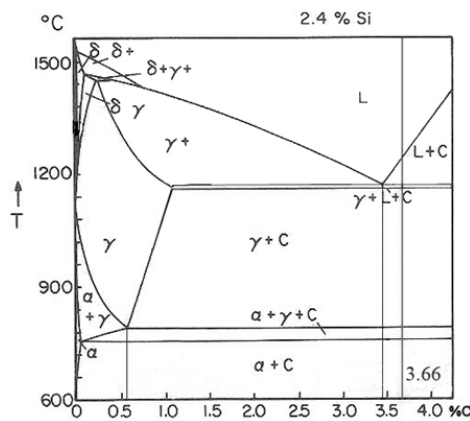


Figure 5: Fe-C diagram for % Si= 2.4 [24].

EXPERIMENTAL RESULTS

3D surface reconstruction procedure allowed to identify a “core zone” in some graphite nodules, with a profile decrease of about $0.5 \mu\text{m}$ (Fig. 6 and 7). Considering largest graphite nodules, “core zone” radius is always lower than the graphite core radius obtained directly from the melt ($C_M + C_E$), but it is necessary to underline that this result was not obtained with all the investigated graphite nodules: some graphite nodules do not show a “core zone” at all.

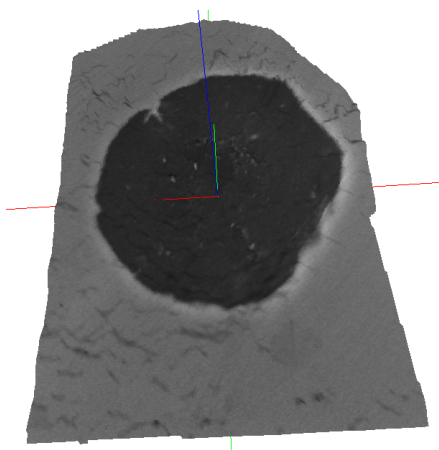


Figure 6: 3D specimen reconstructed surface.

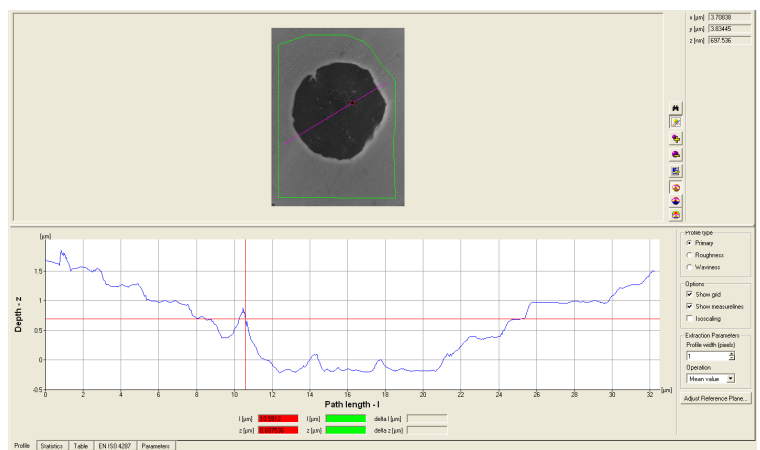


Figure 7: 3D reconstructed specimen. Profile evolution.

Image analysis procedure described in *Material and experimental procedures* works on a matrix of dimension 1120×1600 . As already noted, a preprocessing is advisable and in the chosen application a γ -correction with $\gamma=0.3$ is adopted; the obtained image appear clearer than the original one. In Fig. 8 an original data and its γ -correction are displayed. In Fig. 9



the matrices E , U and C valuated on the specimen of Fig. 8b) and the texture function f are displayed. Note that the “core zone” is enhanced in the texture function, being the clearer elements in the image aside the contour, of course. By thresholding operation (see Fig. 10a) it is possible to identify the “core zone” and characterize this zone by its extension (number of pixels), shape (by the solidity and eccentricity parameters) and location (by its centroid). For the identified zone the area is equal to 136575 pixels, the solidity (that is the ratio between the area and the convex area) is equal to 0.66, the eccentricity is 0.74 and the coordinates of the centroid are (987, 575). In Fig. 10b the contour of the zone identified is shown superimposed to the specimen considered.

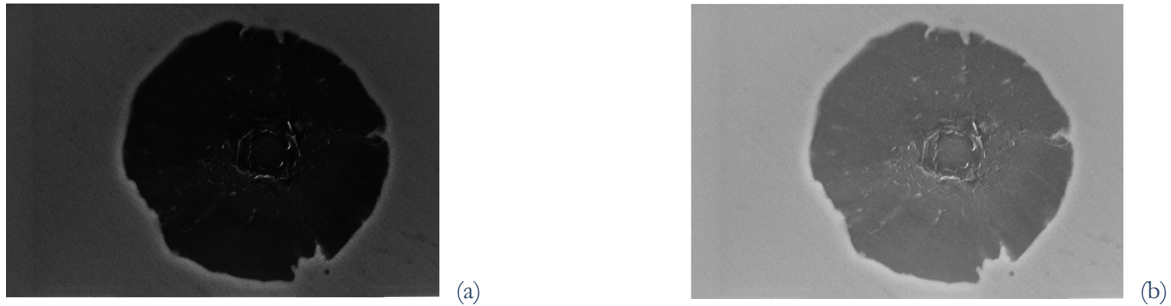


Figure 8: Example of data preprocessing. a) original image; b) data processed by γ -correction with $\gamma=0.3$

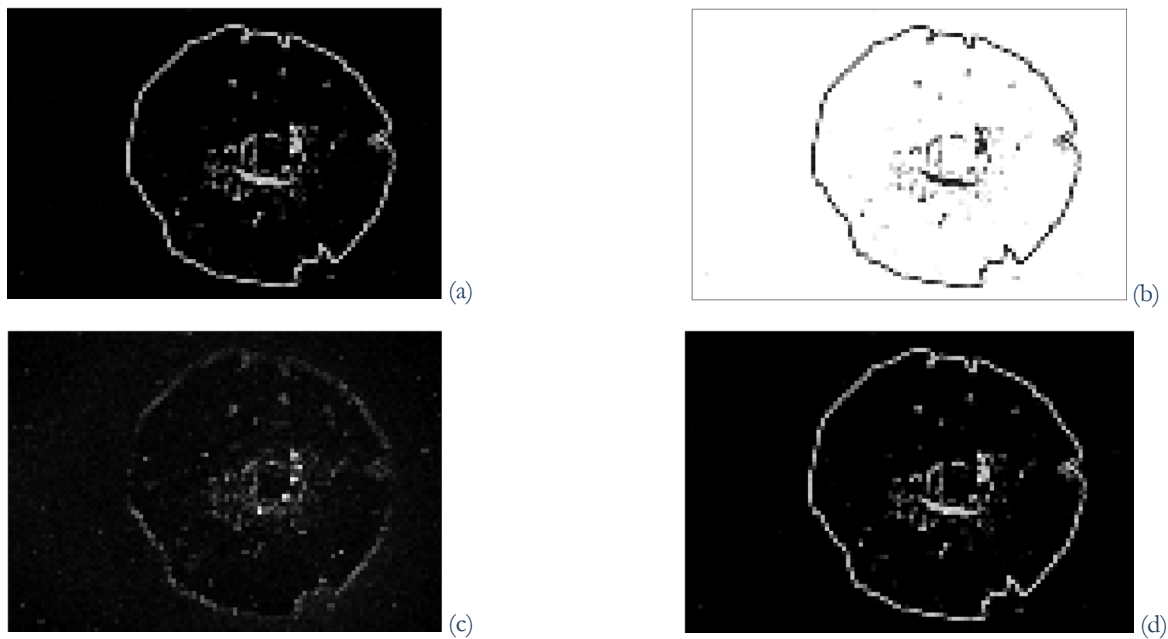


Figure 9: Texture analysis on the data of Fig. 1b. a) Entropy matrix; b) Uniformity matrix; c) Contrast matrix; d) Texture matrix

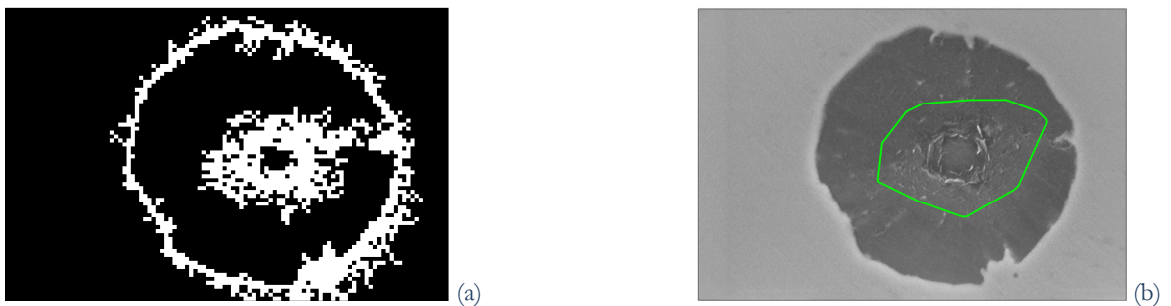


Figure 10: Identification of the “core zone”. a) Threshold operation applied at the texture matrix of Fig. 9d); b) Contour of the identified zone.

This procedure is simpler than the 3D surface reconstruction procedure and does not need a complex experimental preparation. 3D surface reconstruction and the proposed procedure based on image analysis allow to obtain analogous results, both considering qualitatively (identification of the presence of a “core zone”) and quantitatively, with the radius of the “core zone” section that is characterized by the following relationship:

$$R_{Core} \leq R_{C_M + C_E}$$

This result could be associated to three different positions of the metallographic plane respect to the graphite nodule “core” (Fig. 11):

- graphite nodule “core” do not interact with the metallographic plane. As a consequence, no nodule “core” is observed (Fig. 11a);
- graphite nodule “core” is cut by the metallographic plane, not corresponding to the maximum diameter. As a consequence, a nodule “core” could be observed. “Core” and nodule radii relationship in the metallographic plane is: $R_{Core} < R_{C_M + C_E}$ (obviously considering mean values, Fig. 11b);
- graphite nodule is cut by the metallographic plane, roughly corresponding to the maximum diameter. As a consequence, a nodule “core” could be observed, with $R_{Core} \simeq R_{C_M + C_E}$ (considering mean values, Fig. 11c).

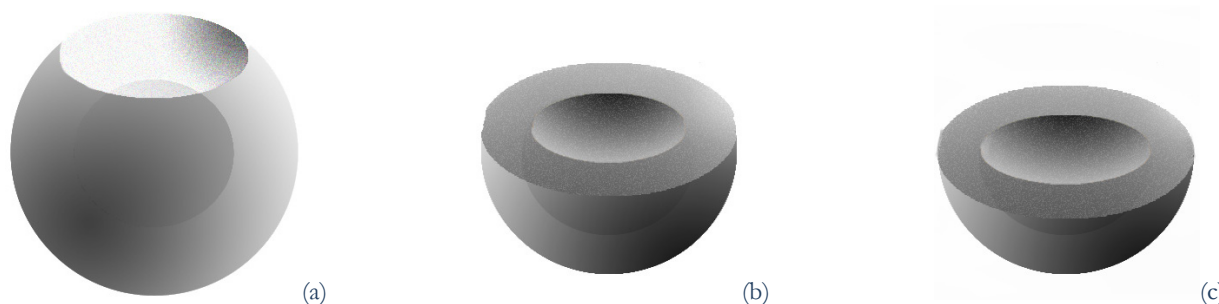


Figure 11: interaction between metallographic plane and graphite nodule (with “core”). a) No metallographic plane – nodule “core” interaction; b) metallographic plane – nodule “core” interaction; c) metallographic plane – nodule “core” interaction corresponding to the maximum diameter.

According to the obtained image analysis results, the graphite nodule “core zone”, characterized by a lower wear resistance, corresponds to the graphite core obtained directly from the melt ($C_M + C_E$). This lower wear resistance probably corresponds to a lower mechanical resistance: as a consequence, the observed disgregation damaging micromechanism that is sometimes observed together to the “onion-like” mechanism could act: cracks nucleate and propagate in nodule center with the stress increase.

CONCLUSIONS

Damaging micromechanisms in DCI are more complex than the simple graphite nodule “debonding” usually considered in numerical simulation as the main damaging micromechanism. Focusing graphite nodules role, the main ferritic DCI damaging micromechanism consists in cracks nucleation and propagation in the graphite shell coming from the reduced carbon solubility in γ phase (“onion-like” mechanism), but a second damaging micromechanism is sometimes observed along with the “onion-like” mechanism: cracks nucleation and propagation in nodule center (“disgregation” mechanism).

In this work, differences in the wear resistance between nodule core and nodule shield were qualitatively evaluated by means of traditional metallographic preparation, both considering a 3D surface reconstruction and performing a customized image processing procedures. Results were compared with the observed damaging micromechanisms, considering the different graphite nodules solidification mechanisms.

3D reconstruction and customized image analysis procedures allow to obtain analogous results, with the second procedure that does not need a complex experimental activity to obtain the images to be analyzed.



On the basis of the experimental results, it is possible to conclude that the graphite core obtained directly from the melt is characterized by a lower wear resistance with respect to the shield zone. Cracks initiation and propagation in the nodule core is probably a consequence of the reduced mechanical resistance.

REFERENCES

- [1] R.G. Ward, An introduction to the physical chemistry of iron and steel making, Arnold, London (1962).
- [2] C. Labrecque, M. Gagne, Canadian Metallurgical Quarterly, 37 (5) (1998) 343.
- [3] M. J. Dong, C. Prioul, D. François, Metall. and Mater. Trans. A, 28A (1997) 2245.
- [4] C. Guillermer-Neel, X. Feaugas, M. Clavel, Metall. and Mater. Trans. A, 31A (2000) 3063.
- [5] J. H. Liu, X. Y. Hao, G. L. Li, G. Sh. Liu, Mater. Letters, 56 (2002) 748.
- [6] R. C. Voigt, L. M. Eldoky, H. S. Chiou, AFS Trans., 94 (1986) 645.
- [7] L. Eldoky, R.C. Voigt, AFS Trans., 86-104 (1986) 631.
- [8] C. Berdin, M. J. Dong, C. Prioul, Engineering Fracture Mechanics, 68 (2001) 1107.
- [9] K. S. Zhang, J. B. Bai, D. François, Int. J. of Solids and Structures, 36 (1999) 3407.
- [10] F. Iacoviello, A. De Santis, D. Iacoviello, O. Di Bartolomeo, In: Convegno Nazionale IGFXIX, Milano, (2007) 10.
- [11] F. Iacoviello, V. Di Cocco, V. Piacente, O. Di Bartolomeo, Materials Science and Engineering A, 478 (1-2) (2008) 181.
- [12] F. Iacoviello, O. Di Bartolomeo, V. Di Cocco, V. Piacente, In: 17th European Conference on Fracture (ECF 17), Brno (CZ), (2008) 52.
- [13] F. Iacoviello, V. Di Cocco, V. Piacente, In: Convegno Nazionale IGFX, (2009) 291.
- [14] F. Iacoviello, V. Di Cocco, In: International Conference on Crack Paths (CP2009), Vicenza (2009).
- [15] V. Di Cocco, F. Iacoviello, M. Cavallini, Engineering Fracture Mechanics, 77 (2010) 2016.
- [16] V. Di Cocco, F. Iacoviello, M. Cavallini, In: 33^o Convegno nazionale AIM, Brescia, (2010) 93.
- [17] Handbook of Medical Imaging: Processing and Analysis Management, Isaac Bankman Editor.
- [18] S. Aramvith, S. Pumrin, T. Chalidabhongse, S. Siddhichai, In: International Symposium on Intelligent Signal Processing and Communication Systems, (2009) 607.
- [19] A. Tripathi, D. Chourshiya, Y. Kumar, In: International Conference on Control, Automation, Communication and Energy Conservation, (2009) 1.
- [20] A. De Santis, O. Di Bartolomeo, D. Iacoviello, F. Iacoviello, J. of Materials Processing Technology, 196 (1-3) (2008) 292.
- [21] V. L. de Araújo Freitas, V. H. C. de Albuquerque, E. de Macedo Silva, A. Almeida Silva, J. M. R.S. Tavares, Materials Science and Engineering A, 527(16-17) (2010) 4431.
- [22] R. C. Gonzales, R. E. Woods Digital Image Processing, Prentice hall Inc.. SMC-3 6 (2002) 610.
- [23] R. M. Haralick, K. Shanmugam, I. Dinstein, IEEE Transactions on Systems, Man , and Cybernetics, SMC-3 (6) (1973) 610.
- [24] I. Minkoff, The physical metallurgy of cast iron, John Wiley and Sons, New York, (1983) 35.